Garg et al., http://www.jgp.org/cgi/content/full/jgp.201210826/DC1

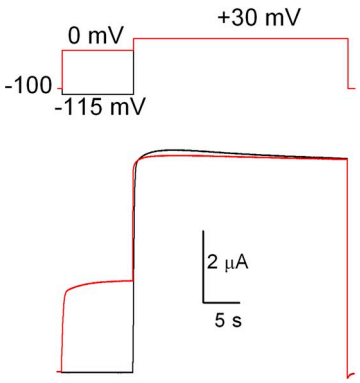

Figure S1. Slow inactivation of WT hEAG1 currents during a long depolarizing pulse. (Top) From a V_h of −100 mV, 10-s V_{pre}s to −115 and 0 mV were applied, each followed by a 30-s-long test pulse to +30 mV. (Bottom) Note that test current elicited after the prepulse to −115 mV was larger than after the prepulse to 0 mV, but that currents relax (inactivate) to a common level by the end of the 30-s test pulse. Traces represent average currents recorded from five oocytes.

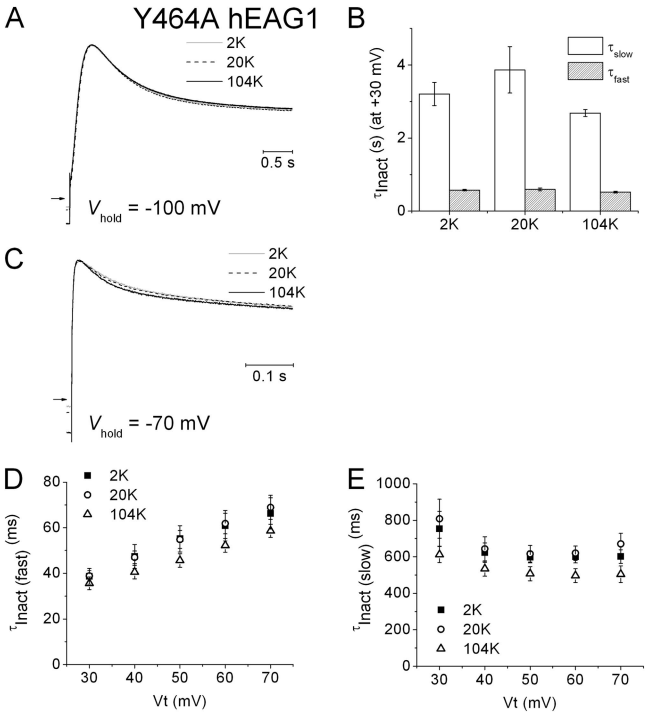

Figure S2. Y464A-induced inactivation in hEAG1 is not slowed by elevated $[K^+]_e$. (A) Normalized and superimposed traces of Y464A hEAG1 currents at +30 mV elicited from a V_h of −100 mV in 2 mM $[K^+]_e$ (gray trace), 20 mM $[K^+]_e$ (dashed trace), and 104 mM $[K^+]_e$ (black trace). (B) Inactivation time constants at +30 mV in different $[K^+]_e$. The decay phase of currents elicited from a V_h of −100 mV was fitted with a two-exponential function (n = 4). There was no significant effect of $[K^+]_e$ on either time constant (P > 0.05). (C) Normalized and superimposed traces of Y464A hEAG1 currents at +50 mV elicited from a V_h of −70 mV in 2 mM $[K^+]_e$ (gray trace), 20 mM $[K^+]_e$ (dashed trace), and 104 mM $[K^+]_e$ (black trace). (D and E) The decay phase of currents at the indicated V_t, elicited from a V_h of −70 mV, was fitted with a two-exponential function to determine inactivation time constants in different $[K^+]_e$ (n = 5). $\tau_{inact(fast)}$ (D) for $[K^+]_e$ of 104 mM was less than $[K^+]_e$ = 2 mM (P = 0.03) or $[K^+]_e$ = 20 mM (P = 0.02). $\tau_{inact(slow)}$ (E) for $[K^+]_e$ of 104 mM was less than $[K^+]_e$ = 2 mM (P = 0.01) or $[K^+]_e$ = 20 mM (P = 0.005).

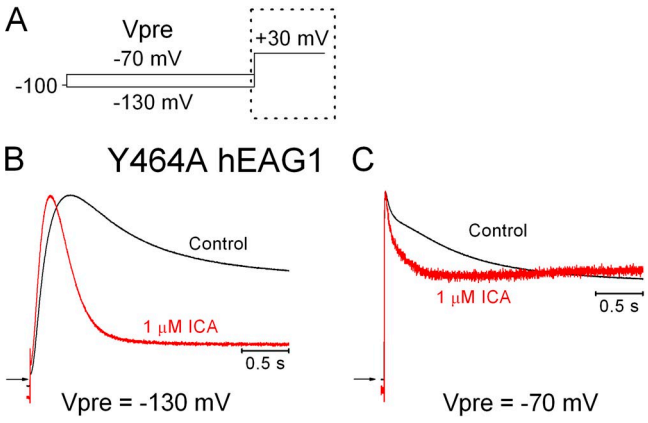

Figure S3. ICA accelerates onset of Y464A hEAG1 current inactivation. (A) Voltage-pulse protocol used to elicit currents plotted in B and C. From a V_h of −100 mV, 10-s V_{pre}s to −130 and −70 mV preceded a 4.5-s test pulse to +30 mV. Currents recorded during the test pulse (boxed region) are shown in B and C. (B) Normalized and superimposed traces of Y464A hEAG1 currents at +30 mV elicited after V_{pre} to −130 mV under control conditions (black trace) and after 1 μM ICA (red trace). (C) Normalized and superimposed traces of Y464A hEAG1 currents at +30 mV elicited after V_{pre} to −70 mV under control conditions (black trace) and after 1 μM ICA (red trace).

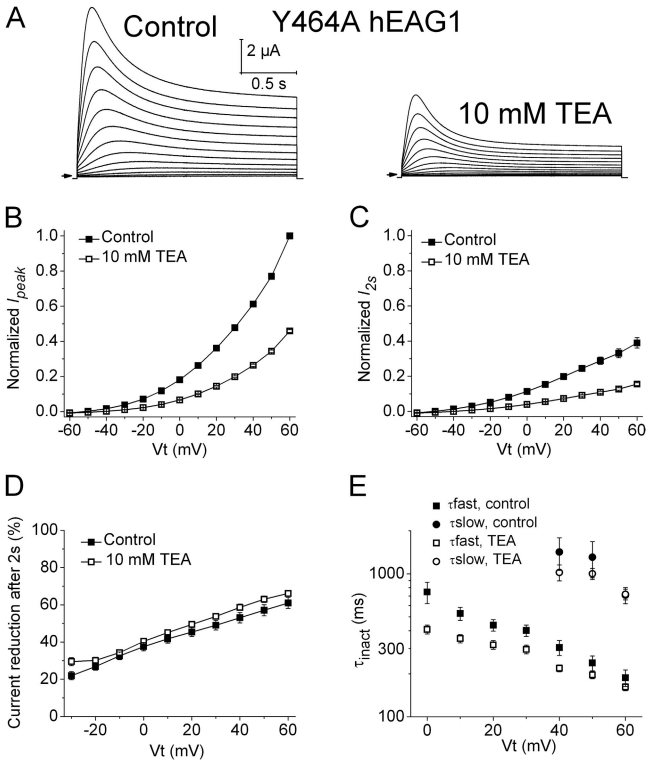

Figure S4. Extracellular TEA blocks Y464A hEAG1 current but does not slow rate of inactivation. (A) Effect of 10 mM TEA on currents elicited with voltage steps varying from −60 to +60 mV in 10-mV increments from a V_h of −100 mV. (B) Normalized peak I-V relationships for hEAG1 channels recorded under control conditions (■) and after the application of 10 mM TEA (□) to the external solution ($n = 9$). (C) Normalized end of 2-s pulse I-V relationships recorded under control conditions (■) and after the application of 10 mM TEA (□; $n = 9$). (D) Voltage-dependent reduction in current amplitude from peak to end of 2-s pulse under control conditions (■) and after the application of 10 mM TEA (□; $n = 9$). (E) Effect of 10 mM TEA on the time constants for onset of inactivation plotted as a function of *V*t. The decay phase of currents elicited from a V_h of −100 mV was fitted with a two- or one-exponential function. TEA accelerated the rate of fast inactivation (two-way ANOVA; $P < 0.0001$). In B–D, the SEM bars are smaller than symbol size.

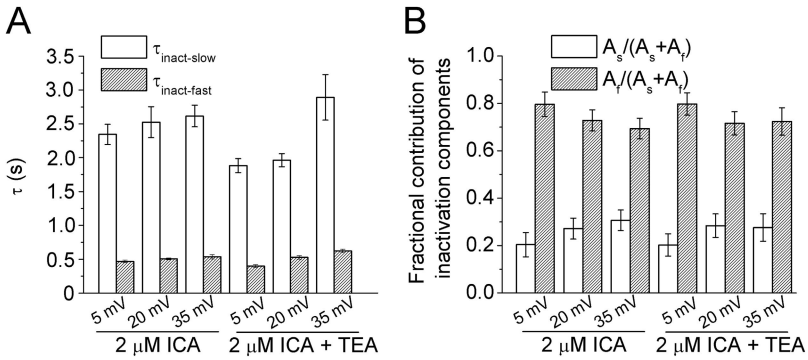

Figure S5. ICA-enhanced inactivation of WT hEAG1 is not slowed by external TEA. (A) Comparison of fast and slow inactivation time constants. The decay phase of currents recorded during a 10-s pulse to +5, +20, and +35 mV was fitted with a two-exponential function to estimate the time constants for inactivation in the presence of 2 μM ICA with and without the coapplication of 10 mM of extracellular TEA. TEA reduced the time constants of inactivation for pulse to +5 mV ($P < 0.05$) but had no effect at other potentials. (B) Comparison of relative amplitudes for fast (A_f) and slow (A_s) components of inactivation at the indicated V_t ($n = 5$).

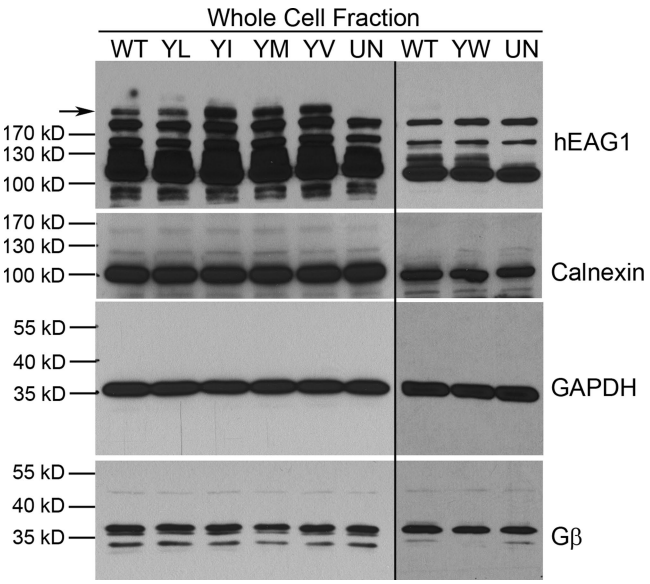

Figure S6. Western blots for hEAG1, calnexin, GAPDH, and Gβ in whole cell fraction of oocytes injected with WT, Y464L (YL), Y464I (YI), Y464M (YM), Y464V (YV), and Y464W (YW) *hEAG1* cRNA, or uninjected (UN). The three right columns are from a different batch of oocytes and different gel. hEAG1 antibody showed reactivity to many intracellular proteins in the whole cell fractions, overlapping the hEAG1 protein (113-kD) signal. A selective high molecular weight signal is visible (denoted by arrow) only in the cRNA-injected groups. Calnexin is an ER protein; GAPDH and Gβ are cytoplasmic proteins.

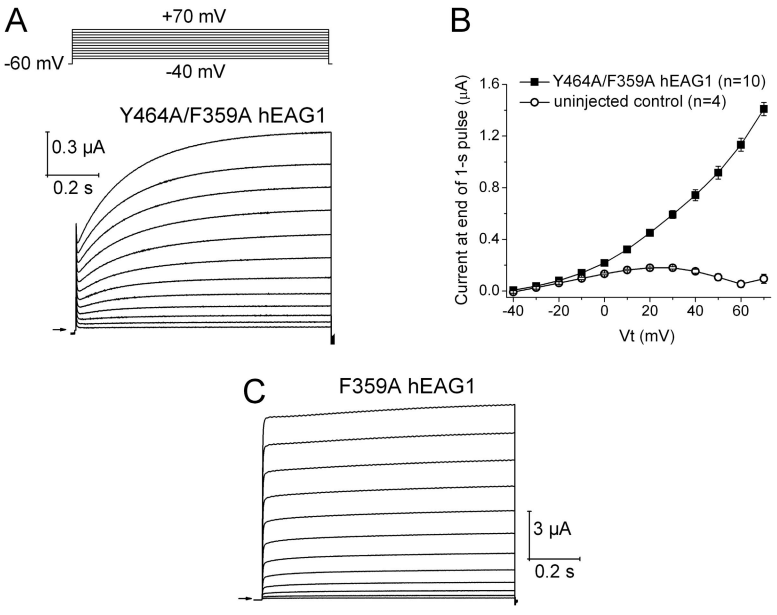

Figure S7. F359A rescues gating of Y464A hEAG1. (A) Voltage-pulse protocol and currents for F359A/Y464A hEAG1 channels. Currents were elicited with 1-s voltage pulses applied in 10-mV increments to a variable V_t. V_h was −60 mV, and the interpulse interval was 15 s. (B) Peak I-V relationship for F359A/Y464A hEAG1 (■) and uninjected control cells (□). (C) Current recordings for F359A hEAG1 using the pulse protocol shown in A.

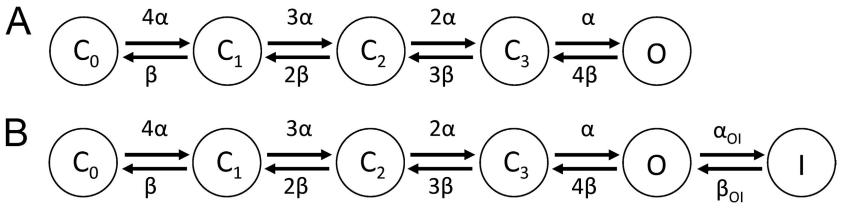

Figure S8. Schematics of simple linear Markov models of EAG1 current. (A) Five-state model. (B) Six-state model.

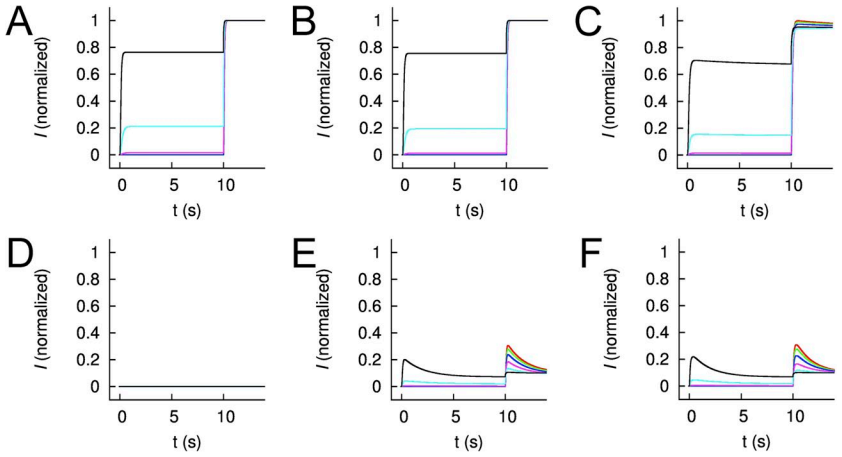

Figure S9. Simulated EAG1 current (I) and effect of ICA determined with different Markov models. In each panel, currents are shown in response to 10-s pulses to a V_{pre} of −130, −100, −70, −40, −10, and +20 mV, followed by a test pulse to +30 mV. (A–C) Simulated control I for 5-, 6-, and 10-state models, respectively. (D–F) Simulated I in the presence of 5 µM ICA for 5-, 6-, and 12-state models, respectively. Color coding of traces is the same as noted in Fig. 11.

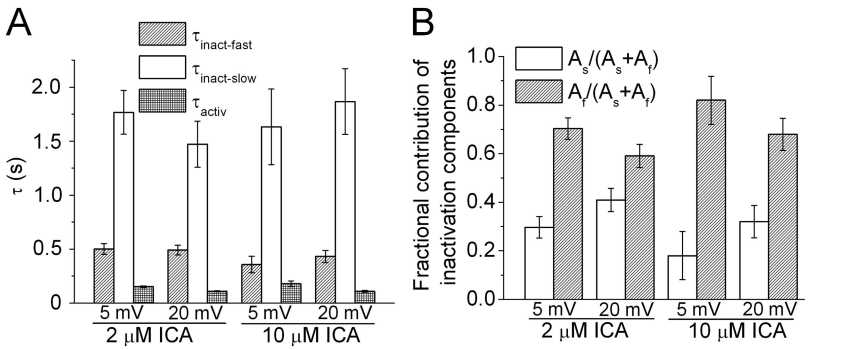

Figure S10. Kinetics of WT hEAG1 channel currents is similar in the presence of 2 or 10 µM ICA. (A) Comparison of activation and inactivation time constants. Currents recorded during 10-s pulses to +5 and +20 mV were fitted with a three-exponential function to estimate a single time constant for the onset of activation and two time constants for onset of inactivation in the presence of 2 or 10 µM ICA (n = 4–5). (B) Comparison of relative amplitudes for fast (A_f) and slow (A_s) components of inactivation at the indicated V_t. [ICA] did not significantly alter any measure of inactivation ($P > 0.05$).

Table S1

Features for model fitting and their fit errors

Feature	Weighting factor	Control	2 µM ICA	5 µM ICA	10 µM ICA	Y464A
$I_{pre\text{-}max}$	1	0.072	0.217	0.448	0.558	0.115
$I_{pre\text{-}end}$	1	0.082	0.479	0.810	0.539	0.108
$\tau_{pre\text{-}slow}$	0.1	0.057	0.061	0.284	0.259	0.068
$\tau_{pre\text{-}fast}$	0.5	0.074	0.137	0.345	0.207	0.098
I_{max}	2	0.267	0.110	0.495	0.552	0.237
I_{end}	2	0.249	0.270	0.251	0.177	0.274
I_{late}	2	0.079	0.002	0.032	0.012	0.012
$\tau_{test\text{-}slow}$	0.25	0.162	0.143	0.198	0.188	0.161
$\tau_{test\text{-}fast}$	0.25	0.222	0.185	0.225	0.223	0.181
$\mathrm{Max}\sum_j \mathrm{C}j$	2	0.004	0.020	0.002	0.011	0.004
$\mathrm{Max}\sum_j \mathrm{O}j$	1	0.189	0.020	0.130	0.006	0.055

$E_i = \left\| f_{m,i} - f_{e,i} \right\|_2 / \left\| f_{e,i} \right\|_2$. Weighting factors were applied to emphasize or deemphasize features. $I_{pre\text{-}max}$, maximal normalized current during prepulse; $I_{pre\text{-}end}$, normalized current at the end of prepulse; $\tau_{pre\text{-}slow}$, slow time constant from biexponential fit of current during prepulse; $\tau_{pre\text{-}fast}$, fast time constant from biexponential fit of current during prepulse; I_{max}, maximal normalized current during test pulse; I_{end}, normalized current at the end of test pulse; I_{late}, normalized current after 20-s test pulse; $\tau_{test\text{-}slow}$, slow time constant from biexponential fit of current during test pulse; $\tau_{test\text{-}fast}$, fast time constant from biexponential fit of current during test pulse.

Table S2

Initial values for models

Models	States	Symbol	Value
5-state	Zeroth closed state	C_0	1
	First–third closed state	C_1, …, C_3	0
	Open state	O	0
6-state	Zeroth closed state	C_0	1
	First–third closed state	C_1, …, C_3	0
	Open state	O	0
	Inactivated state	I	0
10-state	Zeroth closed state	C_0	0.5
	First–third closed state	C_1, …, C_3	0
	Open state	O	0
	Zeroth inactivated state	I_0	0.5
	First–fourth inactivated state	I_1, …, I_4	0
12-state	Zeroth closed state	C_0	0.5
	First–third closed state	C_1, …, C_3	0
	First and second open state	O_1, O_2	0
	Zeroth inactivated state	I_0	0.5
	First–fifth inactivated state	I_1, …, I_5	0

Table S3

Rate constant parameters for models

Parameter	Symbol	Control	2 µM	5 µM	10 µM	Y464A	Unit
Closed–closed and closed–open transitions	α_0	15.620309	10.440446	11.631091	11.148303	6.617790	s^{-1}
	z_α	0.481494	0.533413	0.440578	0.329040	0.600499	
	β_0	13.260124	4.574153	11.332073	11.273359	3.100676	s^{-1}
	z_β	0.004189	0.032021	0.029397	0.007126	0.032085	
Closed–inactivated transitions	α_{CI0}	0.001194	0.001473	0.000004	0.014683	0.002182	s^{-1}
	β_{CI0}	0.086253	0.065298	0.015226	0.027916	0.281901	s^{-1}
	α_{CI1}	0.025614	0.129125	0.164319	0.152015	0.084866	s^{-1}
	β_{CI1}	0.016028	0.077180	0.0442683	0.043349	0.268716	s^{-1}
	α_{CI2}	0.025614	0.256777	0.3286340	0.289347	0.167551	s^{-1}
	β_{CI2}	0.016028	0.089063	0.0733105	0.058782	0.246698	s^{-1}
	α_{CI3}	0.025614	0.384429	0.4929490	0.426679	0.250234	s^{-1}
	β_{CI3}	0.016028	0.100946	0.10235275	0.074215	0.224681	s^{-1}
Open–inactivated transitions	α_{0I}	0.001194	0.512082	0.657264	0.564011	0.332919	s^{-1}
	β_{0I}	0.086253	0.112829	0.131395	0.089648	0.202663	s^{-1}
Open–open transition	λ	0.278176	N/A	N/A	N/A	N/A	s^{-1}
	γ	0.738245	N/A	N/A	N/A	N/A	s^{-1}